Physics – Uspekhi **41** (10) 1015 – 1023 (1998)

REVIEWS OF TOPICAL PROBLEMS PACS numbers: **68.35.p**, **68.55.a**, 81.15.Hi

Monatomic steps on silicon surfaces

A V Latyshev, A L Aseev

Contents

Abstract. The results of studies of monatomic steps on silicon surfaces using *in situ* ultrahigh vacuum reflection electron microscopy are reviewed. The topics covered include the increase in dynamic step edge stiffness under non-equilibrium conditions; step bunch and step antibunch formation processes; electromigration effects; the anomalously high density of Si(111) adatoms; and incipient epitaxial growth.

1. Introduction

Elementary structural processes operating on Si crystal surfaces are of crucial importance in thin-film and other low-dimension technologies, including quantum dots, quantum wires, superlattices and self-organizing adsorbates. Because of the dominant role of Si crystals in today's micro- and nanoelectronics of semiconductors, the basic physical and crystallographic properties of monatomic (one-spacing-high) steps they form are currently a subject of intense research in materials science [1, 2].

Unfortunately, the necessity of using high-resolution electron microscopy in combination with ultrahigh vacuum conditions [3] has for a long time retarded progress in the field, the reason being the film of the natural oxide and impurity adsorbates which, due to their high reaction ability, Si surfaces develop not only under atmospheric conditions but also under the vacuum of 10^{-7} Torr typical of current electron microscopy [4, 5].

Following the experimentation breakthroughs of the 1980s, however, unique and powerful methods have been developed for surface studies, such as scanning tunneling microscopy (STM) [6], reflection electron microscopy (REM) [7 – 9], and low-energy electron microscopy (LEEM) [10, 11], with which the visualization of monatomic steps on Si surfaces became possible. The great appeal of these methods is the possibility of *in situ* experiments, most fully realized in the ultrahigh vacuum reflection electron microscopy (UHV REM) technique.

It is the purpose of this paper to review the author's recent UHV REM investigations into the fundamental aspects of the behavior of monatomic steps on Si surfaces during sublimation, phase transition and epitaxial growth processes.

A V Latyshev, A L Aseev Institute of Semiconductor Physics, Russian Academy of Sciences Siberian Branch
prosp. akad. Lavrent'eva 13, 630090 Novosibirsk, Russia
Tel. (7-3832) 34 40 82, 33 27 66
Fax (7-3832) 33 10 80
E-mail: latyshev@thermo.isp.nsc.ru, aseev@thermo.isp.nsc.ru

Received 26 January 1998
Uspekhi Fizicheskikh Nauk **168** (10) 1117 – 1127 (1998)
Translated by E G Strel'chenko; edited by L V Semenova

2. Reflection electron microscopy

In REM, a beam of high-energy (50 – 100 keV) electrons is directed toward the surface of a bulk crystal at a Bragg angle of a few degrees and the image is formed by electrons elastically scattered onto the aperture diaphragm of the microscope objective lens — an experimental arrangement dating back to the pioneering electron microscopy experiments of the 30s [12]. Since under non-UHV conditions a film of adsorbates and natural oxides develops on a real solid surface and because, further, electrons cannot penetrate more than a few nanometers in this setup, the contrast of the surface image mainly depends on its micro-roughness (the so-called shadow contrast). Because such contrast gives relatively little information about the crystal structure, REM has received little attention as compared with transparent electron microscopy, in which the inner structure of thin crystals or thin replicas of solid surfaces is studied. At the same time, however, due to the microscope column design, with the many movable gaskets needed for tuning the electro-optical system and with high temperatures not allowable, an UHV column has remained a longstanding problem. The use of cryogenic pumping for creating an ultrahigh vacuum in the objective chamber of the transparent microscope enabled further advances in the REM method.

The two most optimum cryogenic UHV REM designs are currently at work in the Tokyo Institute of Technology side entry stage microscope [13] and in its top stage counterpart at

the SB RAS Institute of Semiconductor Physics (Novosibirsk) [14]. In each of these, the cryogenic pump placed in the objective chamber is a closed metal cylinder whose walls are provided with channels for supplying the cooling agent (liquid nitrogen or liquid helium vapor) and with small entrance and exit holes for the electron beam [15].

The sample, a $0.3 \times 1.2 \times 8.0$-mm Si plate cut from a standard single crystal Si wafer, is placed inside the cylinder. The sample is fixed by tantalum holders, is heated by DC, and is free to rotate azimuthally as well as to change its Bragg angle. The design is advantageous in that the sample can be replaced without violating the column vacuum, and that various materials can be deposited onto the sample surface directly in the column by means of a miniature evaporator placed inside the cryogenic pumping device. Further, with REM the electron beam intensity can be measured and the microimages videotaped in the process of an *in situ* experiment.

An atomically clean Si surface is prepared by heating the crystal briefly to 1200 °C [16, 17] thus removing from the surface the natural oxide films and various types of contaminations, mostly Si carbide resulting from the carbon – silicon reaction. A typical REM image of a clean Si(111) surface is shown in Fig. 1. It should be noted that due to the small observation angle the REM image of a surface is shortened by a factor of 30 to 50 along the electron incidence direction and so has different magnifications along and normal to the beam. In Fig. 1, the dark lines are atomic steps and the hatched contrast marked by an arrow at the center of the photo is a dislocation reaching the sample surface. Because the surface-normal component of the dislocation Burgers vector is nonzero, one of the steps breaks at the exit point of the dislocation, implying that the step is monatomic (its height is 0.31 nm). Since all the atomic steps on the surface have the same contrast, it is concluded that all the other steps in Fig. 1 are also monatomic, as the present author and other workers the repeatedly demonstrated by a variety of techniques, such as REM contrast calculation, X-ray data processing, comparing the step velocity and the homoepitaxial Si deposition rate, etc. [14, 16].

The atomic step-dislocation contrast in REM images is a superposition of the diffraction and phase types of contrast [18]. The former, also known as the Bragg type, is due to the fact that deformed regions existing near the monatomic steps change the diffraction conditions locally at the steps. The phase (or Fresnel) contrast relates to the phase shift of the electrons reflected from neighboring atomic planes one monatomic step apart. Due to such superposition, the intensity of a diffracted electron beam is highly sensitive to the structural perfection or otherwise of the crystal lattice near the sample surface. From a comparative contrast analysis of the monatomic steps and lattice deformations around a surface-reaching dislocation, since the deformation field of an individual dislocation is known, it proves possible to estimate the lattice deformation at the steps. It was found to be approximately 2×10^{-4} [19, 14] for monatomic steps on an Si(111) surface.

It should be noted that 0.14-nm-high monatomic steps on an Si(001) surface can be seen in REM images owing to (2×1) and (1×2) superstructure domains alternating on neighboring terraces on either side of the step [20]. The reconstruction of the (001) face is due to atoms with two broken bonds dimerizing along the $\langle 110 \rangle$ direction to form the (1×2) superstructure. In the next (001) atomic plane, one spacing away from the first, dimerization changes its direction by 90°, giving rise to the (2×1) superstructure. Thus, if a plane contains monatomic steps, neighboring terraces in the plane have different superstructure domains, (1×2) and (2×1), the boundary between the two types being the line of a monatomic step on the surface. Using one of the superstructure beams to form the REM image of the stepped (100) surface, one obtains a pattern of alternating bright and dark regions that correspond to various superstructure domains, the boundary between the domains being a monatomic step (Fig. 2). The two types of steps observed at the (001) surface are the smooth boundary going from white on the left to the black on the right (S_A step) and a wiggly boundary in going from black to white (S_B).

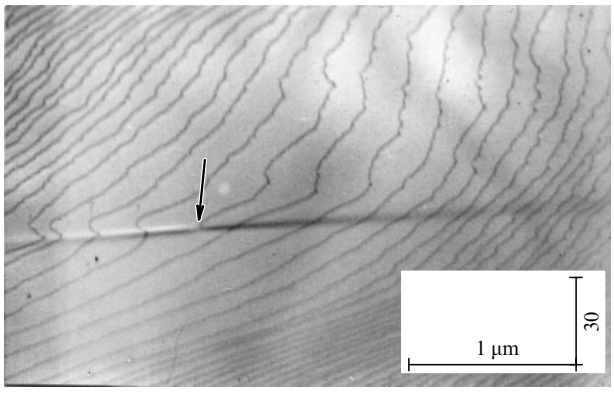

Figure 1. UHV REM image of a stepped Si(111) surface. Dark lines: monatomic steps 0.31 nm in height. Arrow: the dislocation exit point on the surface; the black-and-white image of the surface is due to the sign-alternating elastic deformation field.

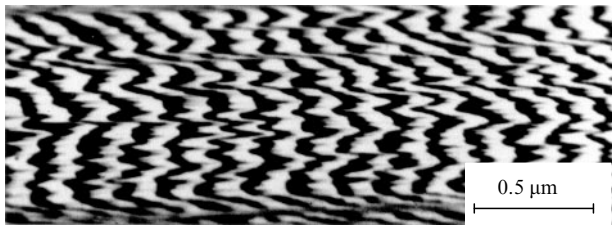

Figure 2. UHV REM image of a Si(111) surface containing a regular system of monatomic steps. The alternation of white and black contrast types is due to the alternation of (2×1) and (1×2) superstructures on the terraces between the steps.

3. Dynamic properties of monatomic steps

As a Si crystal is heated up to 900 °C, adatom generation, displacement, and absorption processes occur at its (111) surface leading to monatomic step shape fluctuations that are detected by *in situ* UHV REM. These fluctuations closely resemble Brownian motion in that both the generation of adatoms (or vacancies) and their absorption by monatomic step edges are random processes [21]. From the balance between thermally activated adatom generation and absorption processes, and using the Langevin's relations to minimize the elastic energy of the curved portions of the steps, the linear tension of the (111) surface steps at thermodynamic equilibrium is found to be $\beta \approx 8 \times 10^{-10}$ J m^{-1} [22].

The linear tension of monatomic steps on the Si(111) surface at nonequilibrium has been examined experimentally by observing the way sublimation-driven monatomic steps interact with points where edge dislocations reach the surface [23]. It is shown that such points act as pinning centers for a moving step and that the detachment of a step from the dislocation occurs when a certain critical curvature of the step is reached (Fig. 3). Note that this experiment yields the reconstruction time of the initial step configuration as a function of crystal temperature, which is essential for achieving smooth surface conditions in molecular mean epitaxy (MBE) technology. In Fig. 4 reproduced from Ref. [24], the amplitude h characterizing the dislocation-induced perturbation of the step shape is shown as a function of time. The relaxation rate $V_{\text{relax}} = \partial h/\partial t$ of the bending of the step following its detachment from the dislocation is described as the difference between the velocity of the straight-line step,

$$V_{\text{step}} = \chi\left(\exp\frac{\Delta\mu}{kT} - 1\right)$$

and that of the bent step,

$$V_{\text{curv}} = V_{\text{curv}}(K, U) = \chi\left(\exp\frac{\Delta\mu}{kT} - \exp\frac{\Omega U}{kT}\exp\frac{\Omega\beta K}{kT}\right),$$

where $\chi = 2\nu\lambda_s \exp(-W/kT)\tanh(d/\lambda_s)$ is the kinetic coefficient, $\Delta\mu$ represents the chemical potential shift, U is the surface energy density due to lattice deformation, λ_s is the adatom diffusion length, W the sublimation energy, T the crystal temperature, d the step separation, Ω the atomic area, ν the atomic frequency, k, Boltzmann's constant, and the step curvature $K = 2h/(h^2 + L^2/4) \approx 8h/L^2$, L being the wavelength of the step bend caused by the interaction with the dislocation. Noting that the bend mainly relaxes far away from the dislocation exit point, we can set $U \approx 0$, which reduces the above equation to the simpler form

$$\frac{\partial h}{\partial t} = \chi\exp\frac{\Omega U}{kt}\exp\left(\frac{\Omega\beta K}{kT} - 1\right).$$

Once the differential equation is solved, the nonequilibrium relaxation of a monatomic step is found to be described by

$$h = h_0\exp\left(-\frac{t}{\tau_{\text{relax}}}\right),$$

where $\tau_{\text{relax}}(T) = kTL^2/8\Omega\chi\beta$ is the relaxation time, h_0 is the step bend at the moment it detaches itself from the pinning center, and t is the time. According to the above expression and the relaxation time data of Fig. 4, the linear tension of monatomic steps on the Si(111) surface increases to $\beta \approx 10^{-9}$ J m^{-1} under high-temperature sublimation conditions.

Thus, in surprising disagreement with theory [25], the dynamic linear tension of Si(111) monatomic steps increases with increasing temperature (Fig. 5). As the crystal temperature is increased, because of the increased number of elemental kinks, the segments of monatomic steps are expected to fluctuate more intensely, making the effective steps wider and, equivalently, the linear tension of the steps less (the width of an effective step means here the average deviation of the segments of a given step from the average position of the step). Above some critical temperature this will result in a morphological transition, 'surface melting' in a sense, where the effective step width becomes infinite. This effect has been observed on many metal surfaces as well as on the Si(001) face [26].

According to Refs [27, 14], one of the reasons why the linear tension of monatomic Si(100) steps increases with temperature is that the step-adatom interaction is anisotropic, i.e., is different for upper and lower terraces (the so-called Schwoebel effect [28]). Evidence for the existence of this effect on Si(111) comes from the measurement of the way the speed of motion of an individual step depends on the width of the upper and lower terraces during sublimation, epitaxy processes, and phase transitions. Taking account of the Schwoebel effect, the step velocity at sublimation under diffusion

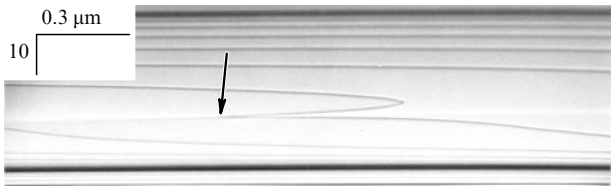

Figure 3. Monatomic step changing shape in passing a dislocation exit point (marked by an arrow) on the Si(111) surface.

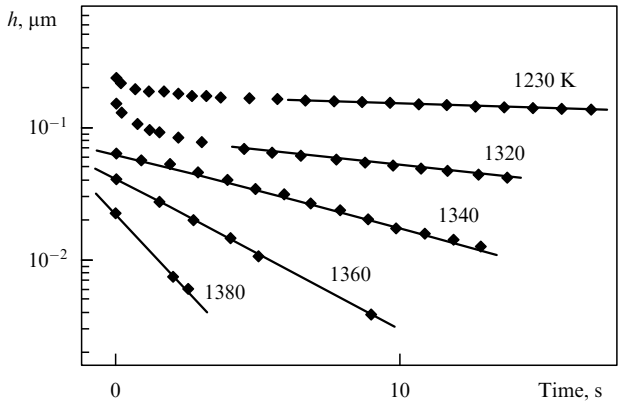

Figure 4. Parameter h characterizing the change of shape of a monatomic step interacting with a dislocation given as a function of time for various temperatures.

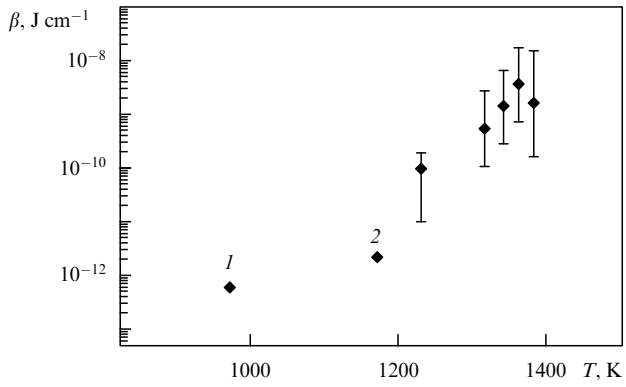

Figure 5. Linear tension of monatomic steps of the Si(111) surface as a function of crystal temperature, including data from the literature: (*1*) Eaglesham D J et al. *Phys. Rev. Lett.* **70** 1643 (1993), (*2*) Alfonso C et al. *Surf. Sci.* **262** 371 (1992).

adatom exchange conditions is given by

$$V = \sigma v \exp\left(-\frac{W}{kT}\right)(\gamma_u d_u + \gamma_l d_l)\,,$$

where $\gamma_{u,l} = \exp(E_{u,l}/kT)$ and $E_{u,l}$ are the probability of existence and the height of the energy barrier to adatom buildup into a monatomic step from the upper (u) and lower (l) terrace; d_u (d_l) is the width of the upper (lower) terrace; and σ is the under-saturation in the vapor phase [29]. From step velocity data, the barrier height difference $\Delta E = E_u - E_l = 0.2 \pm 0.1$ eV is found for adatoms built up into a step from the upper and lower Si(111) terraces. Thus, under sublimation conditions the anisotropy in the adatom-monatomic step interaction coefficients causes steps to smooth up due to the step kinks increasing adatom generation on the lower terrace.

4. Instability of monatomic step systems

In situ REM observations of surface structural processes show that regular systems of monatomic Si(111) and Si(100) steps are unstable under DC heating during the sublimation process. Consequently, regularly arranged monatomic steps transform into bunches of densely spaced steps separated by terraces with a low density of steps [30–32]. Fig. 6 shows REM microphotographs of a Si(111) surface (Fig. 6a) with a regular system of monatomic steps and (Fig. 6b) with a system of step bunches. An very unusual discovery is the existence of fixed sublimation temperature ranges within which the bunching effect is observed. The stability of regular steps in each temperature range depends on the surface electromigration force dependent, in turn, on the direction of the current used to heat the crystal (Fig. 7). Note that in the case of alternating current heating no bunching effect is seen.

A further point to make is that the bunching effect is reversible, that is, step bunches break into a regular array of monatomic steps as the sublimation temperature is changed beyond a bunching temperature range or when it is fixed but the electric current is reversed.

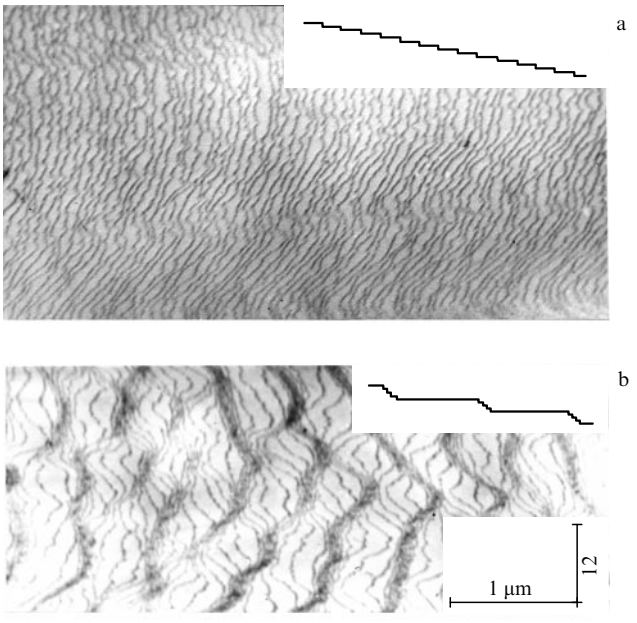

Figure 6. Stepped Si(111) surface for sublimation temperatures of (a) 1270 °C and (b) 1180 °C under step-up DC heating. Insert: schematic of the stepped surface profile.

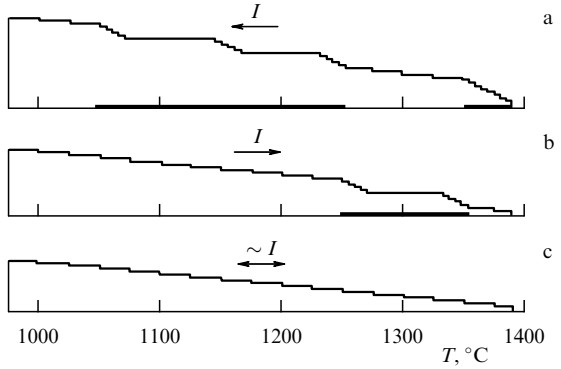

Figure 7. Temperature ranges for the bunching effect on the Si(111) surface during sublimation. The ranges are marked by bold lines on the temperature axis. The arrows in Figs 7a and 7b indicate the direction of the direct current used to heat the crystal; Fig. 7c: heating by AC.

By counting bunch steps and measuring bunch widths it is found that individual monatomic steps in a bunch are a few nanometers apart, i.e., a bunch is not an atomic plane orientated differently from the original surface (facet). For prolonged sublimation, bunches a small distance apart coalesce to form terraces several micrometers wide, the exact width depending on the sublimation temperature and the annealing time. This means that the adatom diffusion length on the Si surface is large under sublimation conditions.

The above aspects of the bunching effect receive some support from studies on the Si(111) step structure using UHV scanning electron microscopy in the reflection regime [33, 34], atomic force microscopy [35], tunneling electron microscopy [36], and synchrotron radiation diffraction [37]. For Si(100), monatomic step bunching is an effect of a more complex nature [38]. First, preceding the bunching process is the pairing of monatomic steps. Second, for a step-up electric current, there is a critical value of the step spacing below which no bunching is observed [32].

The bunching phenomenon has been the subject of extensive theoretical study in recent years. The commonly held view is that it is due to the formation of kinematic, monatomic step density waves that are described by the continuity equation

$$\frac{\mathrm{d}k}{\mathrm{d}t} + c(k)\,\frac{\mathrm{d}k}{\mathrm{d}x} = 0\,,$$

where k is the step density, q the number of steps that pass a given surface point per unit time (step flux), and $c(k) = \mathrm{d}q/\mathrm{d}k$ the kinematic wave velocity, which may or may not be equal to the individual step velocity $v(k) = q/k$. This approach is based on the earlier work of Lighthill and Whitham [39], Chernov [40], and Geguzin and Kaganovskiĭ [41]. Approaching the problem microscopically involves the solution of the well-known Burton–Cabrera–Frank equations [42] for a one-dimensionally moving system of diffusion-coupled monatomic steps with account for adatom drift during electromigration in a DC-heated crystal. Extreme cases arising in this approach have been treated analytically by Stoyanov [43]. A numerical solution of the bunching problem

accounting for elastic step repulsion forces [44 – 46] is based on the well-known work of Marchenko and Parshin [47]. Mention should be made here of attempts to include the anisotropy of adatom migration coefficients, and solutions of the two-dimensional system of step equations of motion within the 'intersecting rays' model [49] should also be noted. Although a great deal of theoretical work has been done on the subject, however, only a qualitative description is at present available for most aspects of the bunching process.

Within the surface electromigration picture the force acting on an adatom may be represented in terms of the Coulomb interaction as

$$F = Z_{\text{eff}} E ,$$

where E is the electric field applied and Z_{eff} the effective adatom charge which may generally be written

$$Z_{\text{eff}} = e(Z_0 - n\sigma_{\text{n}} l_{\text{n}} + p\sigma_{\text{p}} l_{\text{p}}) .$$

where Z_0 is the degree of ionization of the atom; $\sigma_{\text{n,p}}$, $l_{\text{n,p}}$ are the scattering cross section and mean free path of electrons (n) and holes (p), respectively; and e is the electron charge [50]. The first term here is associated with the shell ionization of adsorbed atoms, whereas the two remaining terms account for the dragging of an adatom by directional charge carrier flows in the semiconductor. By comparing experimental data with the theoretically predicted bunching temperatures, the force on an adatom on a DC-heated Si crystal is estimated to be $F \approx 10^{-16}$ N, and the effective Si(111) adatom charge, as $Z_{\text{eff}} \approx 0.1e$ [43]. Generally though, the effective adatom charge is temperature dependent [51].

Recent work of the current authors has shown that bunching on Si surfaces is of an even more complex nature and that for prolonged sublimation times so-called anti-bunches form [52]. These latter are bunches of monatomic steps of opposite sign, which form at some distance from a bunch and are generally of the same shape (Fig. 8).

Antibunch formation is due to the fact that monatomic steps change the direction of their motion during the bunching process, so that the steps move parallel to the bunches. Since bunches significantly affect the distribution of neighboring adatoms, step segments move with different velocities depending on their distances from the bunch, with the ultimate result that monatomic steps develop micro-kinks and that an antibunch parallel to the bunch of the original surface appears.

Since, similar to the bunching effect, antibunching is a reversible process, antibunches decay as the electric current heating the crystal is reversed or as the sublimation temperature changes. Note that a Si surface may undergo very complex micromorphological changes due to the finite values of the bunch (antibunch) formation and decay rates during prolonged annealing under temperature-variable sublimation conditions [53].

5. Monatomic steps at phase transitions

In situ UHV REM experiments [54 – 56] have shown that at a $(1 \times 1) \leftrightarrow (7 \times 7)$ superstructure phase transition the upper edges of Si surface monatomic steps act as initiation centers for (7×7) superstructure domains (Fig. 9). By monitoring the positions of individual monatomic steps during the transition it is found that steps move towards lower lying terraces at the (1×1) to (7×7) transition, i.e., below the transition temperature (about 830 °C), steps move towards lower terraces, whereas at the reverse, (7×7) to (1×1), transition they move towards upper terraces (Fig. 10) [55, 56]. The step displacement is 0.2 to 0.3 times the width of the terraces in-between. Thus, steps absorb surface adatoms when a non-reconstructed (111) (1×1) surface turns into a reconstructed one with a (7×7) superstructure and act as adatom sources for the reverse transition. Two-dimensional growth and evaporation islands change their size in a similar manner at this transition (see Figs 10a, 10b).

The increased intensity of diffracted and mirror reflected electron beams at the transition from reconstructed to non-reconstructed Si(111) implies a more rough non-reconstructed surface, which may indeed be seen from laser ellipsometry data [56]. The important implication is that above the transition the unreconstructed surface temperature is not flat crystallographically but rather contains an anomalously high concentration of adsorbed atoms, corresponding to a monolayer coverage of about 0.2.

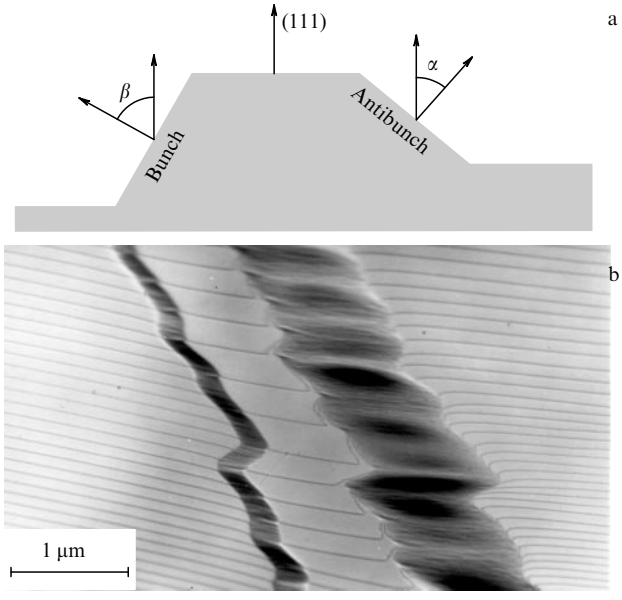

Figure 8. Schematic representation (a) and REM image (b) of the Si(111) surface containing antibunches. The angles α and β for bunches and antibunches are less than one degree.

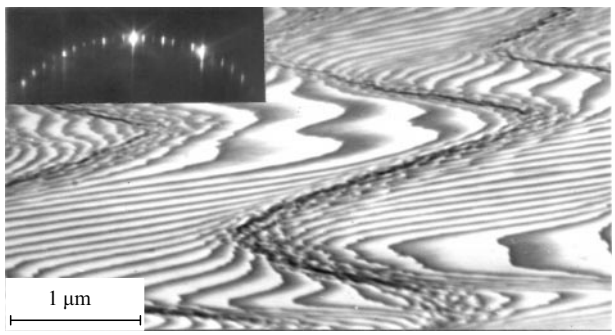

Figure 9. REM image of the stepped Si(111) surface during the $(1 \times 1) \leftrightarrow (7 \times 7)$ superstructure transition. Dark areas: reconstructed surface (1×1). Inset: microdiffraction pattern.

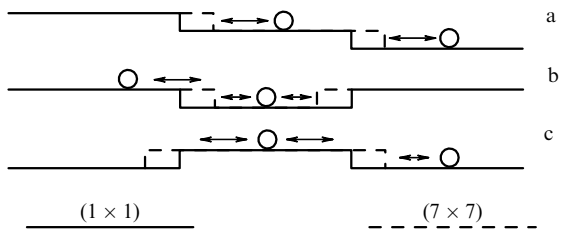

Figure 10. Schematic diagram of reversible monatomic step displacement on a Si(111) surface (a) at the $(1 \times 1) \leftrightarrow (7 \times 7)$ superstructure transition in a regular step system, (b) with a change in the size of a 2D sublimation island, and (c) with a change in the size of a 2D growth island. Solid line: step positions for the (1×1) structure; dashed line: the same for (7×7).

Adding support to this conclusion are electron diffraction intensity calculations for unreconstructed Si(111) [57], which agree with the data best for a surface with a high density of adatoms. Direct evidence for the existence of a disordered layer of mobile adatoms on Si(111) also comes from high-temperature STM studies of the $(7 \times 7) \leftrightarrow (1 \times 1)$ transition [58]. It is noted that the layer of mobile adatoms prevents the visualization of the regular atomic structure of the unreconstructed surface.

The existence of an excess density of adatoms on the unreconstructed relative to the reconstructed (111) surface is also confirmed by an STM study of a Si surface annealed after a fast cooling from above the transition temperature [59]. In this case, along with (7×7) and (11×11) domains, one also observes adatom clustering, due to the fact that adatom absorption by monatomic steps is hampered by the high surface cooling rate and by the low temperatures of the subsequent annealing.

Using the *in situ* UHV REM technique, the reversible transition $(2 \times 1) \leftrightarrow (1 \times 2)$ due to the adatom electromigration effect has been observed on Si(100) [60]. It is shown that the electromigration-driven adatom drift on high mobility terraces (surface atom dimerization initiated by reconstruction is directed parallel to monatomic steps) causes monatomic step pairing, the DC direction determining which surface superstructure, (2×1) or (1×2), is dominant. It is important to note that, analogous to electromigration-induced bunching on (111), (001) monatomic steps do not merge completely when pairing up. This suggests that (100) monatomic steps repel elastically as do their (111) counterparts. This conclusion is confirmed by the STM observation [61] that the mechanical deformation of the crystal affects the dominant type of Si(100) superstructure domains.

6. Epitaxial growth on a silicon surface

In situ UHV REM studies of epitaxial growth present new data on the behavior of monatomic steps during multilayer coating formation. It has been reported [62] that the velocity of monatomic steps during monolayer Ge deposition depends more on the lower than the upper terrace width; the reason being that the energy barrier to a Si adatom building into the step from the lower terrace side is lower than that for the upper terrace. However, epitaxial growth through the building of adatoms into substrate monatomic steps is possible if the adatom diffusion length is greater than the distance to the nearest step, i.e., when the terrace width is less than the critical value $d_c = 2\lambda_s$. Otherwise, 2D growth islands

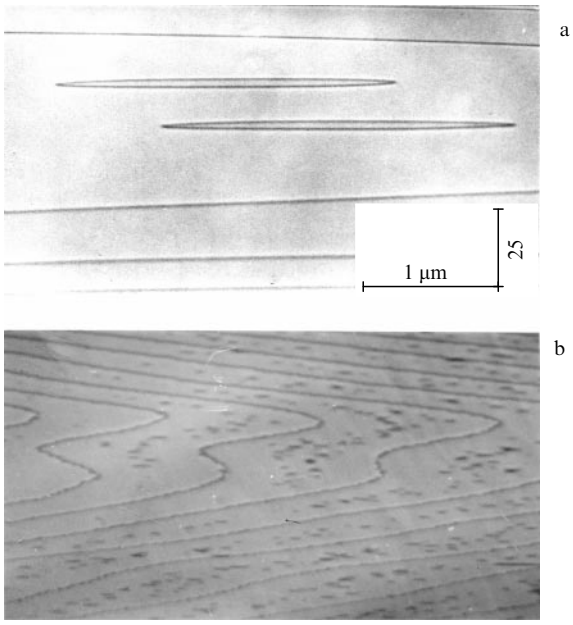

Figure 11. Two-dimensional growth islands on a stepped Si(111) surface at crystal temperatures (a) 950 °C and (b) 850 °C.

form on terraces between steps as shown in Fig. 11, the anisotropy of the coefficients of adatom building into a monatomic step being the reason why the islands are distributed asymmetrically on the terraces.

By applying the UHV REM technique, the critical monatomic step separation at which 2D growth islands start to appear has been measured as a function of the temperature and of the atom deposition flux using the present authors' original techniques in which surface morphology features, bunches and antibunches, are made use of in measuring critical distances (Fig. 12) [63]. The fact that, owing to the attached adatoms, bunches and antibunches slowly approach one another as they counterpropagate makes it possible to determine quite accurately the critical terrace width at which 2D growth islands form. Expressing these results in terms of Arrhenius coordinates one obtains the value of the epitaxial growth activation energy. It is shown that the temperature dependence of the critical separation is characterized by an

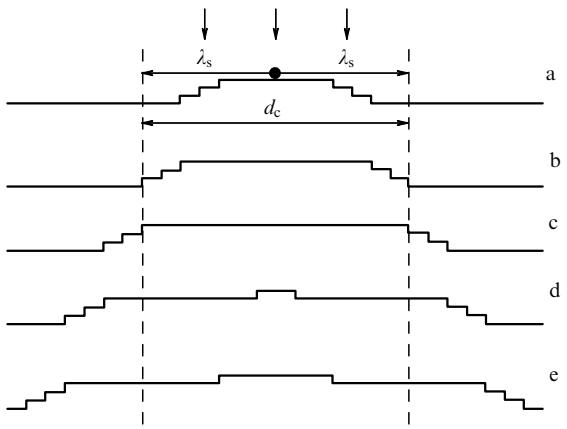

Figure 12. Schematic diagram showing the change in the morphology of a surface containing a bunch and an antibunch during epitaxial growth accompanied with 2D island formation.

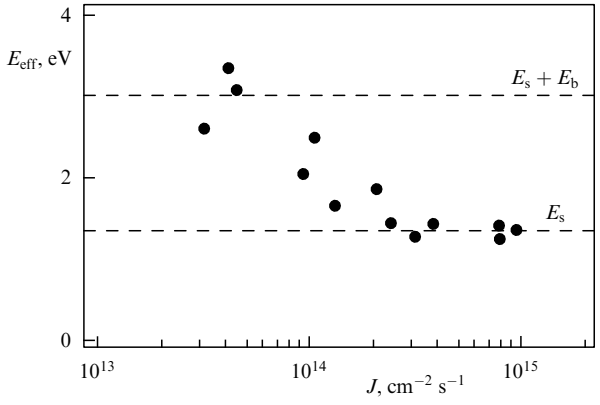

Figure 13. Effective activation energy for the temperature dependence of the critical distance for 2D growth island formation, for various values of adatom flux.

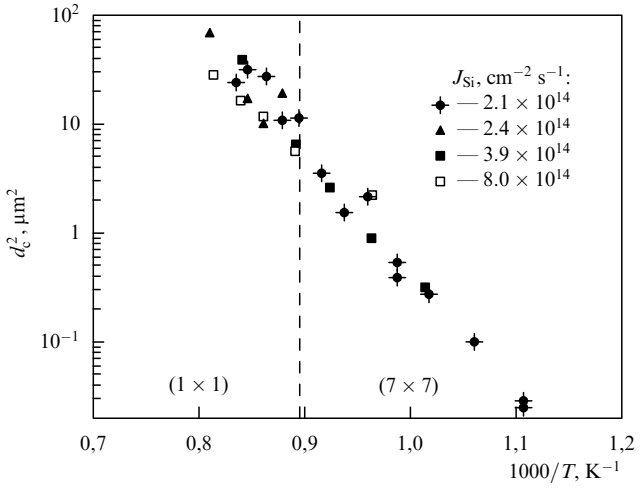

Figure 14. Temperature dependence of the critical distance for epitaxial growth switching from the step-layer to the 2D island nucleation mechanism, for various atomic flux values. The dashed line indicates the $(7 \times 7) \leftrightarrow (1 \times 1)$ transition temperature.

activation energy which depends on the magnitude of the adatom deposition flux (Fig. 13).

It is generally accepted that the adatom diffusion length λ_s is given by the classical Einstein relation

$$\lambda_s^2 = 2D_s\tau_s\,,$$

where $D_s = D_0 \exp(-E_s/kT)$ is the diffusion coefficient of an individual atom, E_s the surface diffusion activation energy for an individual atom, $D_0 = va^2 \exp(S/k)$ the exponential prefactor (with a the atomic separation and S the activation entropy), and τ_s the lifetime of a solitary adatom which for high enough temperatures is determined by adatom desorption from the surface, i.e., $\tau_s = v^{-1} \exp(E_{\text{des}}/kT)$, E_{des} being the desorption energy. For substrate temperatures at which desorption is not important, the lifetime of an adatom depends on its trapping by surface sinks, including the formation of critical size nuclei during the island growth process. The quantity d_c and the number of atoms i in a critical nucleus are related by

$$2\ln d_c \propto \Gamma_{i^*}\left(\ln J^{-1} - \frac{E_{i^*} + E_s}{kT}\right),$$

where $E_{i^*} = E_b(i^* - 1)$ is the adatom binding energy in a critical nucleus of size i^* and the parameter Γ_{i^*} is expressed in terms of the island size as $i^*(i^* + 1)^{-1}$ [64] or $i^*(i^* + 2)^{-1}$ [65]. Note that E_s is uniquely determined by experimental data if $E_{i^*} = 0$, i.e., if the critical nucleus size is $i^* = 1$.

As the critical nucleus size increases, the temperature dependence of d_c is determined by the effective activation energy E_{eff},

$$E_{\text{eff}} = \frac{(E_{i^*}/i^* + E_s)i^*}{i^* + 1}\,.$$

For a large enough number of adatoms in a critical size nucleus ($i^* > 5$) the effective activation energy $E_{\text{eff}} \approx E_b + E_s$. The data of Fig. 13 suggest that for an adatom flow of less than $J^* \approx 3 \times 10^{14}$ cm^{-2} s^{-1} the measured activation energy for the temperature dependence of d_c is a sum of the activation energy for adatom diffusion, $E_s \approx 1.3$ eV, plus the Si binding energy $E_b = 1.7-2.2$ eV. Note that in determining the adatom diffusion length on an Si surface the Einstein relation is only correct when the flow of deposited atoms exceeds $J^* \approx 3 \times 10^{14}$ cm^{-2} s^{-1}, i.e. for large supersaturations. This explains the large spread in the literature values of the adatom diffusion activation energy for the Si surface (see Ref. [63] for a discussion of this point).

Surface reconstruction greatly affects the arrangement of surface atoms and may change the adatom diffusion length. It is therefore of interest to measure the diffusion length on Si(111) near the superstructure transition temperature. Fig. 14 shows *in situ* UHV REM results on the temperature dependence of the critical 2D island formation length for Si epitaxy, including the $(1 \times 1) \leftrightarrow (7 \times 7)$ transition temperature [66]. It is seen that surface superstructure reconstruction does not affect the diffusion length of Si adatoms significantly. Thus, the long-range interaction between surface atoms on a reconstructed surface has little effect on mass transfer on the Si(111) surface.

To conclude this section we should note that at high temperature, i.e., at noticeable adatom desorption levels, an adatom diffusion length of the order of a few millimeters was observed in our experiments (cf. Section 4). This is consistent with the Einstein relation for a large enough pre-exponential D_0 as discussed earlier [67] and so favors the so-called 'long jump' assumption for adatom diffusion along the Si surface, when an elementary adatom jump much exceeds the atomic separation [68].

7. Heteroepitaxy behavior of monatomic steps

UHV REM studies of atomic reconstruction during Ge heteroepitaxy on stepped Si(111) surfaces have shown that the first layers of Ge atoms form in much the same way as in the homoepitaxial case. Ge adatoms build in substrate monatomic steps via the step-layer growth mechanism producing, in so doing, 2D growth islands with terraces narrower than the critical value $d_c = 2\lambda_s$; the temperature dependence of the Ge adatom diffusion length λ_s showing the activation energy $E_s \approx 1.2$ eV [69]. From the reflection high electron diffraction (RHEED) phase diagram, the Si(111) surface coated by Ge displays a superstructure whose

particular type depends on the temperature and the amount of Ge deposited [70]. By controlling the formation of fractional Ge monolayers on stepped Si(111), one can fulfil the necessary conditions for obtaining regular lateral superlattices in which strips of fractional Ge and those of Si surface alternate along monatomic steps.

The main obstacle to the formation of lateral superlattices when Ge submonolayers are deposited on a Si surface is that monatomic steps on the substrate cluster as a polycentric pattern of Ge induced reconstructed domains start to appear. Fig. 15 is a schematic representation of the step clustering process. If the boundary of a surface-propagated superstructure domain meets a monatomic step as it moves along the Si surface, from this moment the boundary and the step move as a whole until they come across another such monatomic step. As a result, the steps that dominate the surface are several atomic separations in height, that is, the surface relief is rough as compared to the regular arrangement of monatomic steps on the original vicinal surface. The morphological transition just described is reversible, the clustered steps breaking into individual monatomic steps as a reverse superstructure transition takes place [71, 72].

Monatomic step clustering during the polycentric nucleation of superstructure domains with mass transfer between monatomic steps has also been observed with UHV REM for gold, calcium, and copper deposited on the Si (111) surface. In these observations, a strong redistribution of substrate monatomic steps near the boundaries of superstructure domains should be noted. The study of the formation of Ca-induced (3×1) domains has shown that due to the adatom electromigration both the domain shape and the cluster configuration of monatomic steps on the surface depend significantly on the DC direction [73].

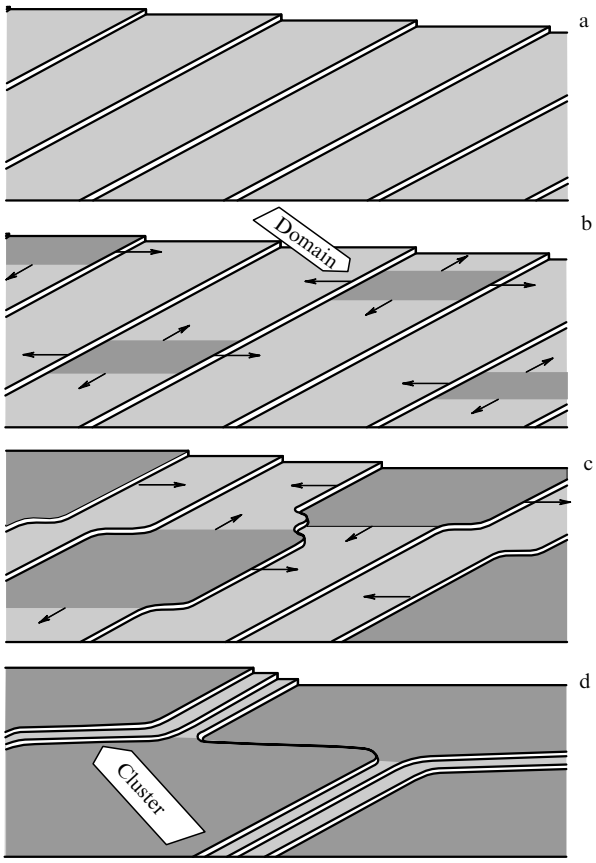

Figure 15. Schematic diagram showing successive monatomic step clustering stages on Si surfaces during the formation and growth of impurity-induced superstructure domains (shown dark).

8. Conclusions

In situ UHV REM studies have shown that monatomic steps on Si surfaces exhibit a number of unusual properties, such as elastic deformation; pairing on the (100) surface; displacement at a superstructure phase transition on the (111) surface; the increase of dynamic linear strain with increasing temperature under sublimation conditions; clustering during the formation of impurity-induced superstructure domains; and finally, the instability of a system of monatomic steps towards the bunch and antibunch formation due to adatom electromigration.

The great advantage of the UHV REM technique is that from the analysis of monatomic step behavior, quantitative characteristics of surface atomic processes may be determined, among them the quasi-equilibrium time parameter, the adatom concentration and diffusion length. An important application of the effects described here is the non-lithography formation of various kinds of self-organized systems on vicinal silicon surfaces, such as ordered systems of step bunches, lateral surface superlattices, strips of impurity-induced superstructures running along step bunches, etc.

Acknowledgements

The authors gratefully acknowledge the contribution of the untimely deceased Professor S I Stenin to the development of the UHV REM technique and its application to fundamental research. Our original works were co-authored with A B Krasilnikov, L V Litvin, L V Sokolov, and D A Nasimov of the SB RAS Institute of Semiconductor Physics, and with K Yagi, H Minoda, and Y Tanishiro (Tokyo Institute of Technology), to all of whom the authors gratefully acknowledge their indebtedness.

This research was supported by RFBR grants and by the RF Science and Technology Ministry "Surface Atomic Structures" program (Grant No. 2-15).

References

1. Rzhanov A V *Elektronnye Protsessy na Poverkhnosti Poluprovodnikov* (Electronic Processes on Semiconductor Surfaces) (Moscow: Nauka, 1971)
2. Hasegawa S, Ino S *Int. J. Mod. Phys. B* **7** 3817 (1993)
3. Bechstedt F, Enderlein R *Semiconductor Surfaces and Interfaces: Their Atomic and Electronic Structures* (Physical Research, Vol. 5) (Berlin: Akademie-Verlag, 1988) [Translated into Russian (Moscow: Mir, 1990)]
4. Nesterenko B A, Snitko O V *Fizicheskie Svoĭstva Atomarno-Chistoĭ Poverkhnosti Poluprovodnikov* (Physical Properties of Atomically Clean Semiconductor Surface) (Kiev: Naukova Dumka, 1983) [Translated into English (Moscow: Nauka, 1988)]
5. Nesterenko B A, Lyapin V G *Fazovye Perekhody na Svobodnykh Granyakh i Mezhfaznykh Granitsakh v Poluprovodnikakh* (Transitions on Free Faces and Phase Interfaces in Semiconductors) (Kiev: Naukova Dumka, 1990)
6. Wiesendanger R, Guntherodt H-J (Eds) *Scanning Tunneling Microscopy* III (Berlin, New York: Springer-Verlag, 1993)
7. Kondo Y et al. *Ultramicroscopy* **35** 111 (1991)
8. Aseev A L, Latyshev A V, Stenin S I, in *Electron Microscopy* Vol. 2 (Budapest, 1984) p. 1215
9. Uchida Y, Lehmpfuhl G *Surf. Sci.* **188** 364 (1987)

10. Bauer E et al. *Ultramicroscopy* **31** 49 (1989)
11. Telieps W, Bauer E *Surf. Sci.* **162** 163 (1985)
12. Ruska E *Z. Phys.* **83** 492 (1933); Ruska E *Nobel Lecture* (Stockholm, 8 December, 1986) [*Usp. Fiz. Nauk* **154** 243 (1988)]
13. Takayanagi K et al. *J. Phys. Sci. Instrum.* **11** 441 (1978)
14. Aseev A L, Latyshev A V, Stenin S I, in *Problemy Elektronnogo Materialovedeniya* (Problems in Electronic Materials Science) (Novosibirsk: Nauka, 1986) p. 109
15. Latyshev A V, Krasil'nikov A B, Vyrypaev B A, Aseev A L, USSR Certificate of Authorship No. 1772702, priority date 1 January 1990
16. Osakabe N et al. *Surf. Sci.* **97** 393 (1980)
17. Ishikawa Y et al. *Surf. Sci.* **159** 256 (1985)
18. Wang Z L *Reflection Electron Microscopy and Spectroscopy for Surface Analysis* (Cambridge, New York: Cambridge Univ. Press, 1996) p. 430
19. Yagi K *Surf. Sci. Rep.* **17** 305 (1993)
20. Latyshev A V et al. *Surf. Sci.* **227** 24 (1990)
21. Alfonso C et al. *Surf. Sci.* **262** 371 (1992)
22. Bartelt N C et al. *Phys. Rev. B* **48** 15453 (1993)
23. Latyshev A V et al. *Phys. Rev. Lett.* **76** 94 (1996)
24. Latyshev A V et al. *Jpn. J. Appl. Phys.* **34** 5768 (1995)
25. Nozieres P, in *Solids Far from Equilibrium* (Ed. C Godreche) (Cambridge, New York: Cambridge Univ. Press, 1991) p. 1
26. Bartelt N C, Tromp R M, Williams E D *Phys. Rev. Lett.* **73** 165 (1994)
27. Uwaha M, Saito Y, Sato M *J. Cryst. Growth* **146** 164 (1995)
28. Schwoebel R L, Shipsey E J *J. Appl. Phys.* **37** 3682 (1966)
29. van Leeuwen C, van Rosmalen R, Bennema P *Surf. Sci.* **44** 213 (1974)
30. Latyshev A V et al. *Dokl. Akad. Nauk SSSR* **300** 84 (1988) [*Sov. Phys. Dokl.* **33** 352 (1988)]
31. Latyshev A V et al. *Surf. Sci.* **213** 157 (1989)
32. Litvin L V, Krasilnikov A B, Latyshev A V *Surf. Sci. Lett.* **244** L121 (1991)
33. Stoyanov S, Nakahara H, Ishikawa M *Jpn. J. Appl. Phys.* **33** 254 (1994)
34. Homma Y, Suzuki M *Appl. Surf. Sci.* **60/61** 479 (1992)
35. Suzuki M et al. *Appl. Surf. Sci.* **60/61** 460 (1992)
36. Tokumoto H, Iwatsuki M *Jpn. J. Appl. Phys.* **32** 1368 (1993)
37. Ramstad M J et al. *Europhys. Lett.* **24** 653 (1993)
38. Latyshev A V, Litvin L V, Aseev A L *Appl. Surf. Sci.* (1998) (in press)
39. Lighthill M J, Whitham G B *Proc. R. Soc. London Ser. A* **229** 281 (1955)
40. Chernov A A *Usp. Fiz. Nauk* **73** 277 (1961) [*Sov. Phys. Usp.* **4** 116 (1961)]
41. Geguzin Ya E, Kaganovskiĭ Yu S *Diffuzionnye Protsessy na Poverkhnosti Kristalla* (Diffusion Processes on Crystal Surface) (Moscow: Energoatomizdat, 1984)
42. Burton W K, Cabrera N, Frank F C *Philos. Trans. R. Soc. London Ser. A* **243** 299 (1951)
43. Stoyanov S *Jpn. J. Appl. Phys.* **29** L659 (1990); *Appl. Surf. Sci.* **60/61** 55 (1990); *Jpn. J. Appl. Phys.* **30** 1 (1991)
44. Natori A, Fujimura H, Fukuda M *Appl. Surf. Sci.* **60/61** 85 (1992)
45. Natori A, Fujimura H, Yasunaga H *Jpn. J. Appl. Phys.* **31** 1164 (1992)
46. Yasunaga H, Natori A *Surf. Sci. Rep.* **15** 205 (1992)
47. Marchenko V I, Parshin A Ya *Zh. Eksp. Teor. Fiz.* **79** 257 (1980) [*Sov. Phys. JETP* **52** 129 (1980)]
48. Krug J, Dobbs H T *Phys. Rev. Lett.* **73** 1947 (1994)
49. Kandel D, Weeks J D *Phys. Rev. Lett.* **69** 3758 (1992); **72** 1678 (1994); **74** 3632 (1995)
50. Fiks V B *Fiz. Tverd. Tela* (Leningrad) **1** 1321 (1959)
51. Kandel D, Kaxiras E *Phys. Rev. Lett.* **76** 1114 (1996)
52. Latyshev A V, Krasilnikov A B, Aseev A L *Ultramicroscopy* **48** 377 (1993)
53. Latyshev A V, Krasilnikov A B, Aseev A L *Surf. Sci.* **311** 395 (1994)
54. Tanishiro Y, Takayanagi K, Yagi K *Ultramicroscopy* **11** 95 (1983)
55. Latyshev A V, Aseev A L, Stenin S I *Pis'ma Zh. Eksp. Teor. Fiz.* **47** 448 (1988) [*JETP Lett.* **47** 530 (1988)]
56. Latyshev A V et al. *Surf. Sci.* **254** 90 (1991)
57. Kohmoto S, Ichimiya A *Surf. Sci.* **223** 400 (1989)
58. Iwatsuki M et al. *Appl. Surf. Sci.* **60/61** 580 (1992)
59. Yang Y-N, Williams E D *Phys. Rev. Lett.* **72** 1862 (1994)
60. Latyshev A V et al. *Pis'ma Zh. Eksp. Teor. Fiz.* **48** 484 (1988) [*JETP Lett.* **48** 526 (1988)]
61. Webb M et al. *Surf. Sci.* **242** 23 (1991)
62. Latyshev A V et al. *Phys. Status Solidi A* **113** 421 (1989)
63. Latyshev A V, Krasilnikov A B, Aseev A L *Phys. Rev. B* **54** 2586 (1996)
64. Stoyanov S *J. Cryst. Growth* **94** 751 (1989)
65. Venables J A, Spiller G D T, Hanbucken M *Rep. Prog. Phys.* **47** 399 (1984)
66. Latyshev A V, Krasilnikov A B, Aseev A L *Phys. Status Solidi A* **146** 251 (1994)
67. Alfonso C, Heyraud J C, Metois J J *Surf. Sci. Lett.* **291** 745 (1993)
68. Senft D C, Ehrlich G *Phys. Rev. Lett.* **74** 294 (1995)
69. Latyshev A V, Krasilnikov A B, Aseev A L *Thin Solid Films* **281/282** 20 (1996)
70. Lamin M A et al. *Surf. Sci.* **207** 418 (1989)
71. Aseev A L, Latyshev A V, Krasilnikov A B *J. Cryst. Growth* **115** 393 (1991)
72. Krasilnikov A B et al. *J. Cryst. Growth* **116** 178 (1992)
73. Krasilnikov A B, Latyshev A V, Aseev A L *Surf. Sci.* **290** 232 (1993)